SUPPLEMENTARY INFORMATION

Finding the Equilibrium of Organic Electrochemical Transistors

Vikash Kaphle[1], Pushpa Raj Paudel[1], Drona Dahal[1], Raj Kishen Radha Krishnan[1] & Björn Lüssem[1,2]

[1]*Department of Physics, Kent State University, Kent, OH, 44242, USA*

[2]*Corresponding Author,* `blussem@kent.edu`

Supplementary Information

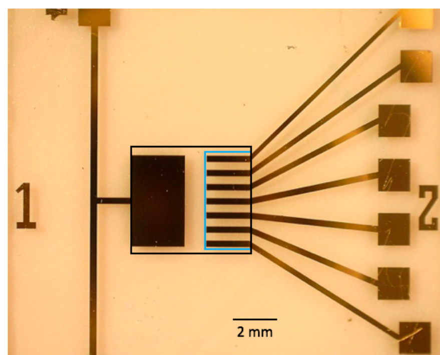

Supplementary Figure 1 Transistor geometry used to study the potential inside the OECT channel. The blue rectangle marks the area, where the channel consisting of PEDOT:PSS is deposited, and the black rectangle represents the part of the device that will be covered by the electrolyte. The left electrode is used as gate, whereas the electrodes on the right are used either as source and drain electrodes or as voltage probes.

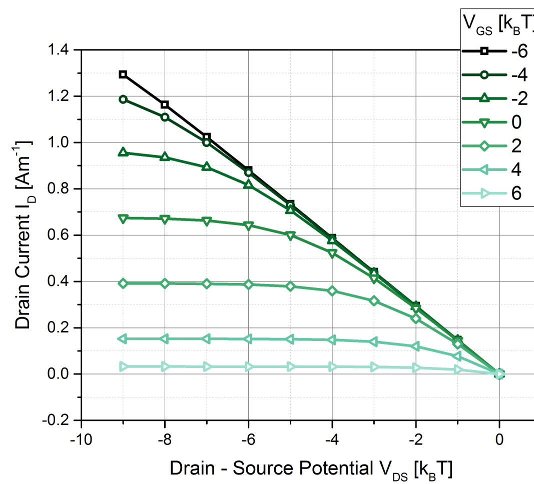

Supplementary Figure 2 Output characteristic. Calculated output characteristic of the OECT shown in Figure 6. Simulation parameters are summarized in Supplementary Table 1.

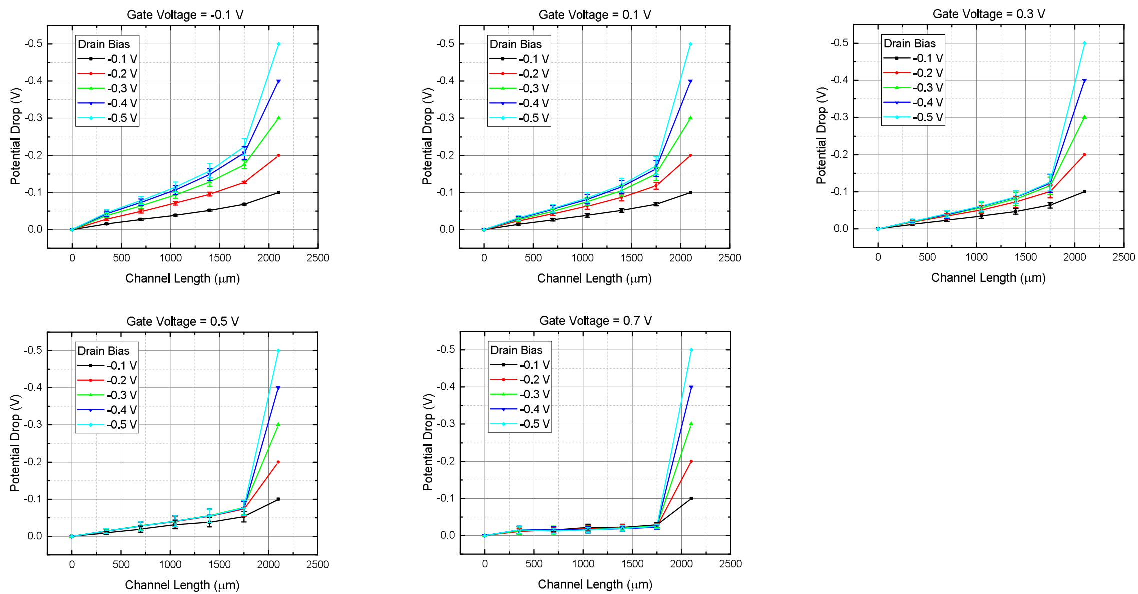

Supplementary Figure 3 Channel potential. Potential inside the transistor channel for all drain and gate potentials.

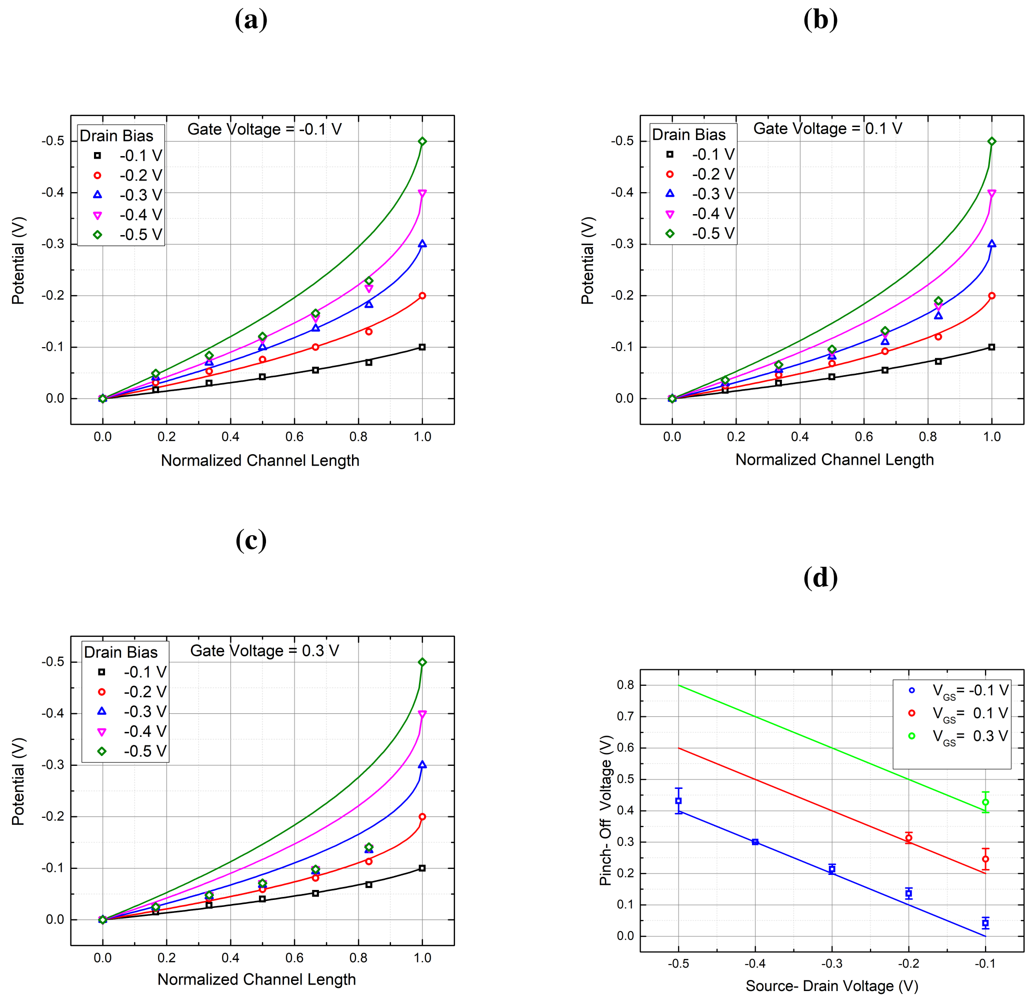

Supplementary Figure 4 Fitting assuming a constant mobility. Channel Potential profile $\Phi(x')$ fitted using Equation 8, i.e. for a constant mobility. **a.** to **c.** show the fit for $V_{\text{GS}} = -0.1V, 0.1V, 0.3V$. **d.** Average pinch-off voltage V_{P} extracted from fitting of the channel potential profile.

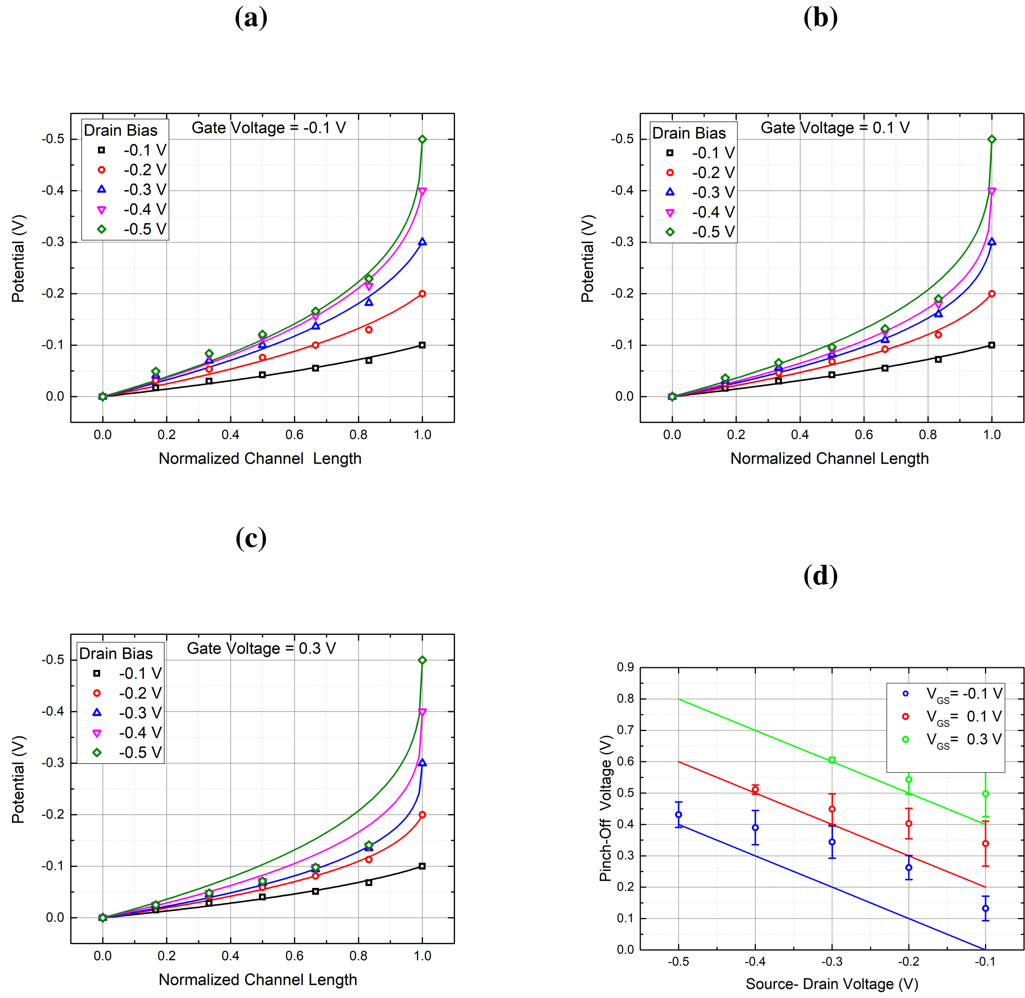

Supplementary Figure 5 Fitting assuming charge carrier dependent mobility. Channel Potential profile $\Phi(x')$ fitted using Equation 9, which takes a dependency of the charge carrier mobility on the hole concentration into account. **a.** to **c.** show the fit for $V_{\mathrm{GS}} = -0.1V, 0.1V, 0.3V$. **d.** Average pinch-off voltage V_{P} extracted from fitting the channel potential profile.

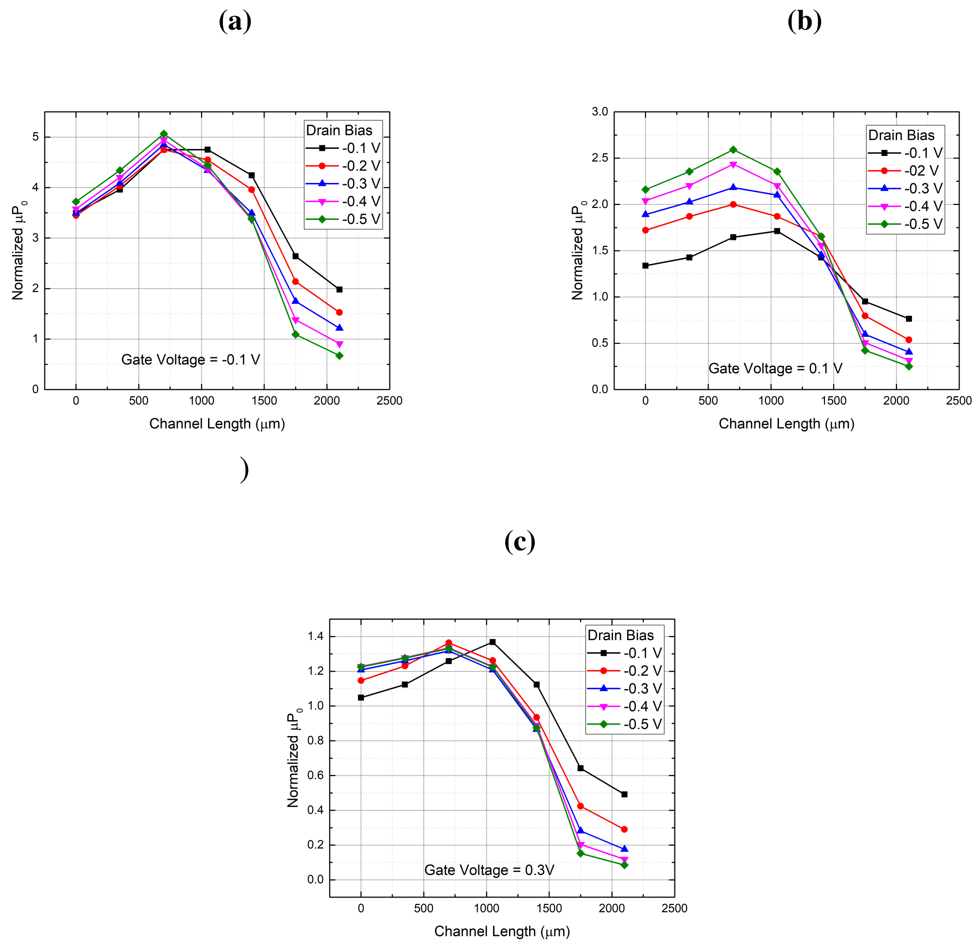

Supplementary Figure 6 Concentration of holes along the channel. Product of hole concentration and hole mobility along the transistor channel for (**a.** to **c.**) $V_{\mathrm{GS}} = -0.1V, 0.1V, 0.3V$.

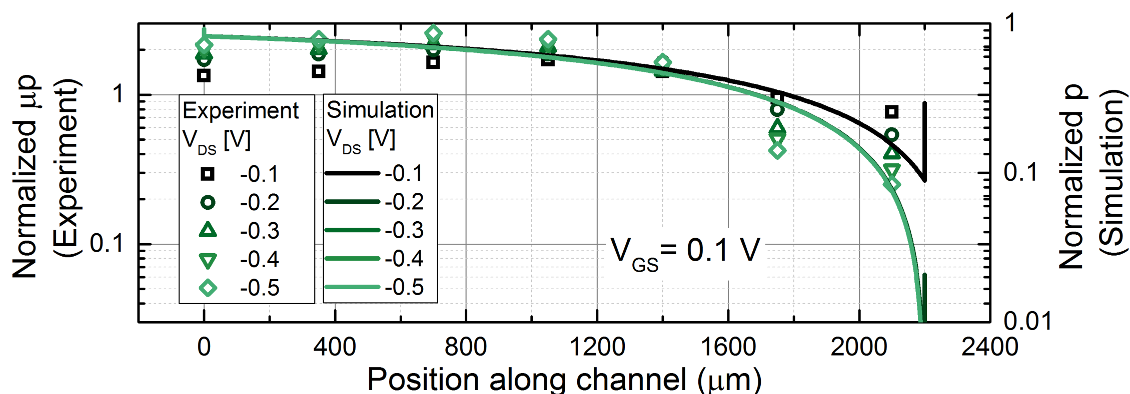

Supplementary Figure 7 Concentration of holes along the channel. Comparison of the normalized product $p(x)\mu(x)$ derived from the experiment (symbols) with the hole concentration $p(x)$ obtained from the 2D model (lines). The parameters listed in Supplementary Table 2 are used for the calculation.

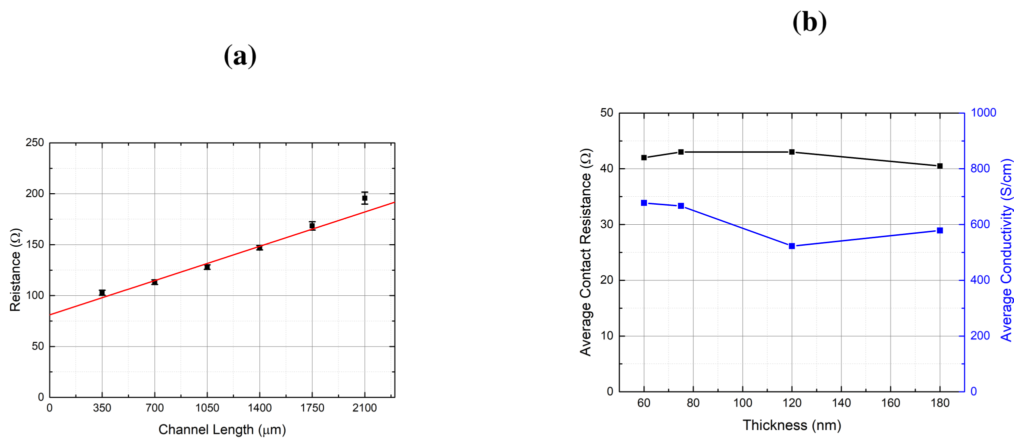

Supplementary Figure 8 Contact resistance. a. Transmission line method to extract contact resistance and conductivity of PEDOT:PSS. **b.** Contact resistance and conductivity of PEDOT:PSS with respect to thickness of the PEDOT:PSS film.

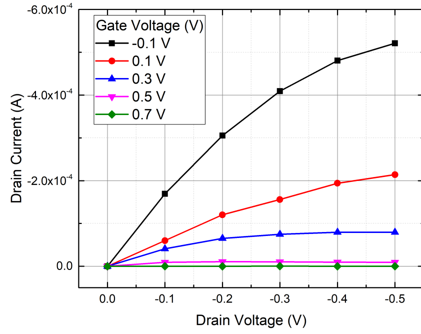

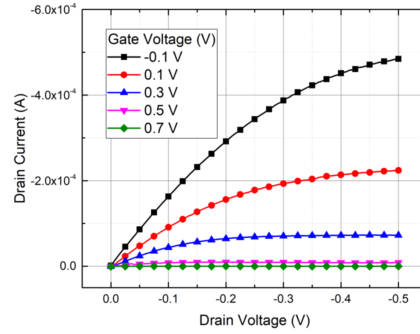

.

Supplementary Figure 9 Verification of measurement setup. Comparison between the output characteristics (a) extracted current flowing in the channel from the four probe method to measure potential, and (b) from standard drain sweep measurements.

Doping Concentration p_0 $[cm^{-3}]$	Ion Concentration N_0 $[cm^{-3}]$	Hole Mobility μ_{p} $[cm^2(Vs)^{-1}]$	Cation Mobility $\mu_{\text{p,ion}}$ $[cm^2(Vs)^{-1}]$
10^{20}	10^{18}	10^{-1}	10^{-4}

Dielectric Constant ϵ	Thickness PEDOT:PSS d_{PEDOT} $[nm]$	Thickness Electrolyte $d_{\text{Electrolyte}}$ $[nm]$	Channel Length L $[\mu m]$
3	31.2	10	1.13

Supplementary Table 1 Model parameters used for short channel OECTs. Parameters used for the simulation of OECTs shown in Figure 6.

Channel Length L $[\mu m]$	Doping Conc. p_0 $[cm^{-3}]$	Ion Conc. N_0 $[cm^{-3}]$	Hole Mob. μ_p $[\frac{cm^2}{Vs}]$	Contact Resistance R_C $[\Omega]$	Cation Mob. $\mu_\mathrm{p,ion}$ $[\frac{cm^2}{Vs}]$
350 , 700, 1050 1400, 1750, 2100	10^{21}	10^{20}	0.2	40	10^{-4}

Channel Length L $[\mu m]$	Dielectric Const. ϵ	Thick. PEDOT:PSS d_PEDOT $[nm]$	Thick. Electrolyte $d_\mathrm{Electrolyte}$ $[nm]$	$\Delta\mu$ $[V]$
350 , 700, 1050 1400, 1750, 2100	3	120	54	0.4, 0.38, 0.31 0.22, 0.15, 0.08

Supplementary Table 2 Model parameters used for long channel OECTs. Parameters used for the simulation of OECTs with varying channel length shown in Figure 8. A small contact resistance was added (cf. Supplementary Figure 8). Furthermore, a difference between the chemical potential of the gate electrode and the source/drain electrode $\Delta\mu$ was assumed.

9 **Supplementary Note 1: Calculation of Channel Potential $\Phi(x)$ and hole concentration $p(x)$**
10 **from Bernards model[1]** The channel potential inside the channel $\Phi(x)$ can be derived from Equa-
11 tion 4 or the main manuscript, but integrating from source to a point x along the transistor channel
12 instead of integrating from source to drain. This leads to (cf. ref. [2]):

$$\int_0^x j dx = \int_0^{\Phi(x)} -ep(x)\mu(x) d\Phi \quad (1)$$

$$I_\mathrm{D} x = \frac{GLV_\mathrm{P}}{\frac{E_0}{k_\mathrm{B}T}+1}\left\{\left[1-\frac{V_\mathrm{GS}-V_\mathrm{DS}}{V_\mathrm{P}}\right]^{\frac{E_0}{k_\mathrm{B}T}+1} - \left[1-\frac{V_\mathrm{GS}}{V_\mathrm{P}}\right]^{\frac{E_0}{k_\mathrm{B}T}+1}\right\} \quad (2)$$

13 with $G = p_0 e \mu_0 \frac{wd}{L}$. For $\frac{E_0}{k_\mathrm{B}T} = 1$ (i.e. for a constant mobility μ, one obtains

$$\Phi(x') = V_\mathrm{GS} - V_\mathrm{P} + \sqrt{\frac{2I_\mathrm{D}V_\mathrm{P}}{G}x' + (V_\mathrm{P} - V_\mathrm{GS})^2}, \quad (3)$$

14 where $x' = \frac{x}{L}$. From Equation 6, one finds that $\frac{I_\mathrm{D}V_\mathrm{P}}{G} = \left(V_\mathrm{P} - V_\mathrm{GS} + \frac{V_\mathrm{DS}}{2}\right) V_\mathrm{DS}$, which is used in
15 Supplementary Equation 3 to arrive at Equation 8.

16 Similarly, one obtains for $\frac{E_0}{k_\mathrm{B}T} = 2$

$$\Phi(x') = V_\mathrm{GS} - V_\mathrm{P} + \sqrt[3]{\frac{3I_\mathrm{D}V_\mathrm{P}^2}{G}x' + (V_\mathrm{P} - V_\mathrm{GS})^3}, \quad (4)$$

17 which, using Equation 5, can be simplified to Equation 9.

18 Similarly, one can obtain the hole concentration as a function of x, as already presented by
19 Friedlein et al. [2]

$$\frac{p(x)}{p_0} = \left\{\frac{I_\mathrm{D}\left(\frac{E_0}{k_\mathrm{B}T}+1\right)x}{GLV_\mathrm{P}} + \left(1-\frac{V_\mathrm{GS}}{V_\mathrm{P}}\right)^{\frac{E_0}{k_\mathrm{B}T}+1}\right\}^{\frac{k_\mathrm{B}T}{E_0+k_\mathrm{B}T}} \quad (5)$$

20 **Supplementary Note 2: Determination of hole concentration along the channel.** As discussed
21 in the main text, the density of free holes and the charge carrier mobility $p(x)\mu$ can be determined

22 from Ohm's law $j = -ep(x)\mu\frac{d\Phi(x)}{dx}$ and the experimental measurement of $\Phi(x)$ (cf. Supplementary
23 Figure 6).

24 Assuming that the variation of the hole mobility μ along the channel is small, the normalized
25 hole concentration $\frac{p(x)}{p_0}$ is proportional to $1 - \frac{p_{\text{ion}}(x)}{p_0}$, i.e. any accumulation of ions at the electrodes
26 will be visible as drop in the hole concentration.

27 Indeed, it is found that the product of mobility and hole density decreases at the drain con-
28 tact, which resembles the trend seen in the simulation (Figure 7). In Supplementary Figure 6 an
29 accumulation of holes is visible not only at the drain, but to a lesser extend at the source electrode
30 as well. This observation can be explained by the negative potential difference between source and
31 gate and, consequently, by an accumulation of ions at the source due to this potential difference
32 and consequently a vertical electric field.

33 **Supplementary Note 3: Gradual channel approximation and OECTs.** In deriving Equations 5
34 and 6, the gradual channel approximation was used implicitly. The gradual channel approximation
35 states that the charges in the channel are solely controlled by the vertical electric field E_y generated
36 by the gate potential [3]. In other words, the lateral electric field E_x is assumed to be much smaller
37 than the vertical electric field E_y, which implies as well that $\frac{\partial E_x}{\partial x} \ll \frac{\partial E_y}{\partial y}$. Using the gradual channel
38 approximation, the two dimensional Gauss' law can be reduced to a 1D equivalent

$$\frac{\partial E_x}{\partial x} + \frac{\partial E_y}{\partial y} \approx \frac{\partial E_y}{\partial y} = \frac{\rho(x,y)}{\epsilon}, \tag{6}$$

39 where $\rho(x, y)$ is the charge density. Supplementary Equation 6 is the justification that the den-
40 sity of free charge carriers inside the channel can be calculated from the difference between the
41 gate potential and the channel potential at position x of the channel only. One obtains for p-type
42 transistors that

$$p(x) = \frac{C_{\text{ox}}}{e} \left(V_{\text{GS}} - \Phi(x) \right), \tag{7}$$

43 with C_{ox} the gate capacitance.

44 Equation 1 used to derive Equations 5 and 6 was proposed to resemble Supplementary Equa-
45 tion 7. However, in contrast to standard thin-film theory, Equation 2 enforces that the film is
46 electrically neutral, i.e. $\rho(x, y) = 0$. Therefore, Gauss' law becomes

$$\frac{\partial E_x}{\partial x} + \frac{\partial E_y}{\partial y} = \frac{\rho(x, y)}{\epsilon} = 0, \tag{8}$$

47 Furthermore, it has been reported that OECTs depend on the thickness of the PEDOT:PSS layer,
48 i.e. the transconductance of the device scales with the volume of the PEDOT:PSS layer. This
49 observation indicates that the electrical potential does not vary along the vertical axis of the device.
50 One obtains

$$\frac{\partial E_x}{\partial x} + \frac{\partial E_y}{\partial y} \approx \frac{\partial E_x}{\partial x} = 0. \tag{9}$$

51 Therefore, the lateral electric field inside the channel is expected to be constant, i.e. the potential
52 along the channel rises linearly, which is indeed observed in the numerical model.

53 Overall, it is uncertain if the gradual channel approximation can be applied to OECTs. In the
54 second part of the manuscript, Gauss' law is solved without a-priory invoking the Gradual Channel

Approximation, which makes the conclusion drawn from the improved model more reliable. However, for the first part of the manuscript, Equation 5 and 6 can be seen as first-order approximation of the problem under the assumption of a de-doping process described by Equation 2.

Supplementary Note 4: Drift-Diffusion Simulation Model The drift-diffusion model used here is based on a Finite Difference discretization scheme, which solves Poisson's equation

$$\nabla^2\Phi(x,y) = \frac{e}{\epsilon\epsilon_0}\left(-p(x,y) - p_{\text{ion}}(x,y) + p_0(y) + N_0(y)\right), \quad (10)$$

and the continuity equations for holes and cations in steady state

$$\nabla\left[e(q\mu_{\text{q}}\vec{\mathbf{E}} - D_{\text{q}}\nabla q)\right] = 0 \quad (11)$$

where q can represent holes p or cations p_{ion}. Doping inside the PEDOT:PSS layer is treated by assuming dopant saturation, i.e. all dopants are assumed to be activated. Interactions between cations, holes, and PSS^- is modeled by electrostatic interactions only. All variables $(j, p, n, p_{\text{ion}}, x, y)$ are normalized internally, improving the convergence of the code at high charge carrier concentrations and large electric field observed in the space charge layers.

The three differential equations are solved self-consistently following the Gummel Method. To increase stability, Poisson's equation was adapted as originally proposed by Gummel

$$\nabla^2\Phi(x,y) = -\frac{e}{\epsilon\epsilon_0}\left(\left[\frac{p^k + p^k_{\text{ion}}}{V_{\text{T}}}\left(\Phi^{k+1} - \Phi^k\right)\right] - p^k(x,y) - p^k_{\text{ion}}(x,y) + p_0(y) + N_0(y)\right), \quad (12)$$

where the superscript k and $k+1$ denotes the solution of the kth or $k+1^{th}$ iteration. Please note that the original Poisson Equation is recovered for convergence of the device, i.e. if $\Phi^{k+1} = \Phi^k$.

70 Boltzmann statistics is assumed throughout the device, which allows to relate the diffusion
71 constant and mobility of holes and ions by the Einstein Equation. Anions in the electrolyte and
72 PSS^- ions are assumed to be stationary.

73 For results shown in Figure 8, the continuity equation of cations was not solved directly,
74 but the ion concentration was calculated according to Equation 15, which enforces a zero ion
75 current throughout the device. In some cases the results were checked against a full simulation,
76 i.e. a simulation in which the continuity equation for cations is solved explicitly. Furthermore, the
77 results shown in Figure 6 and 7 were obtained by a full simulation of the device.

78 **Supplementary Note 5: Contact Resistance of OECTs.** The arrangement of source/drain elec-
79 trodes as shown in Supplementary Figure 1 allows to determine the contact resistance of PE-
80 DOT:PSS even without a gate electrode connected. Here, we process the PEDOT:PSS channel at
81 varying spin coating speed (ranging from 1000 rpm to 4000 rpm), leading to a varying layer thick-
82 ness (from $180\mu m$ to $80\mu m$ verified by optical profilometry). The resistance of each PEDOT:PSS
83 layer before application of the electrolyte is plotted with respect to the channel length in Supple-
84 mentary Figure 8a for a 180 nm thick PEDOT:PSS film. Supplementary Figure 8a can be fitted by
85 a linear function; its slope can be used to determine the conductivity of the PEDOT:PSS formula-
86 tion used here, whereas the intercept represents the combined contact resistance at the source and
87 drain electrode. The contact resistance is found to be approximately equal to $R_{\mathrm{C}} = 80\Omega$.

88 In Supplementary Figure 8b, the average conductivity and contact resistance are plotted with
89 respect to film thickness. It is found that the contact resistance is independent of the film thick-

90 ness. Furthermore, the contact resistance represents a significant fraction of the total resistance.
91 In particular for the smallest channel length of $350\ \mu m$, the contact resistance accounts for about
92 $42 \pm 2\Omega$ of the total resistance.

93 As expected, the conductivity of the films before application of the electrolyte does not de-
94 pend on the film thickness as well. Overall, the conductivity of the PEDOT:PSS mixed with do-
95 deycelbenzene sulfonic acid (DBSA) and ethylene glycol (EG) is in the range of $611 \pm 73 S/cm$
96 which is comparable to other literature results[4].

97 **Supplementary Note 6: Verifying the measurement setup.** The transistor arrangement as shown
98 in Supplementary Figure 1 can be used to measure the potential inside the transistor channel, if the
99 outer two contacts are used as source and drain contacts and the potential at the electrodes in
100 the middle are used to measure the potential with respect to the source electrode. However, the
101 additional electrodes inside the channel region might change the transistor behavior, for example
102 by changing the distribution of ions inside the channel. To test if this is really the case, we extract
103 the current flowing in the channel at a particular drain and gate bias while measuring the channel
104 potential (shown in Supplementary Figure 9a) and compare it to a standard output characteristic
105 (shown in Supplementary Figure 9b). Both measurements are almost identical, which indicates the
106 transistor behavior is not influenced by the additional sense electrodes within the channel, i.e. the
107 measurement is not falsified.

108 **Supplementary Note 7: Calculation of the hole and cation concentration.** The hole concen-
109 tration plotted in Figure 4a was calculated using Equation 7 of the publication of Friedlein et al.[2]

110 (cf. Supplementary Equation 5), assuming a constant charge mobility (i.e. $\frac{E_0}{k_\mathrm{B}T} = 1$). From the
111 hole concentration, the normalized cation concentration is calculated using Equation 2. Finally,
112 the electric field is calculated from the derivative of the potential along the channel $E_x = -\frac{d\Phi}{dx}$.
113 The potential was calculated using Equation 8.

114 **Supplementary References**

115 116 1. Bernards, D. & Malliaras, G. Steady-state and transient behavior of organic electrochemical
117 transistors. *Advanced Functional Materials* **17**, 3538 (2007).

118 2. Friedlein, J. T., Shaheen, S. E., Malliaras, G. G. & McLeod, R. R. Optical measurements
119 revealing nonuniform hole mobility in organic electrochemical transistors. *Advanced Electronic*
120 *Materials* **1**, 1500189 (2015).

121 3. Sze, S. & Lee, M. *Semiconductor Devices* (John Wiley & Sons, Inc, 2012).

122 4. Khodagholy, D. *et al.* High transconductance organic electrochemical transistors. *Nature Com-*
123 *munications* **4**, 2133 (2013).